INTERSECTION OF AN OBLIQUE SHOCK WAVE WITH A CYLINDRICAL AFTERBODY*

G C Shen
Luoyang Dynamics Institute
People's Republic of China

and

D R Philpott
The Hatfield Polytechnic
United Kingdom

Abstract

Surface pressure distributions, oil film and schlieren photographs have been obtained for the intersection of a cylinder by a weak oblique shock wave, (generated by wedges giving flow deflections of 6°, 9.5° and 13°) in a free stream Mach number of 2.5. The effect of the cylinder nose length and the position of the wedge were investigated.

1. Introduction

In high performance military aircraft shock waves generated by different components frequently impinge on neighbouring surfaces with significant effect. Consequently, the study of localised shock reflections and boundary layer interactions are of great importance and a considerable number of investigations have been made (e.g. Refs. 1, 2 and 3). The bulk of this work has, however, been concerned with two dimensional interactions and a relatively small number with three dimensional interactions of practical interest, such as the intersection of a fin generated shock wave with a fuselage boundary layer (Ref. 1).

The present investigation is concerned with the particular interaction problem associated with the carriage of stores, and is a development of work previously reported in Ref. 2. The situation considered is the effect of an oblique shock wave, generated as the bow wave of a store, or by another aircraft component, as it interacts with the boundary layer on the afterbody of a neighbouring store, such as a missile.

In order to gain an understanding of the flow field, as well as to provide data which would be applicable to a range of practical solutions, it was decided to simplify the interaction by considering a plane shock wave intersecting a long cylindrical afterbody, well away from the influence of the nose.

The experiment is similar to that of Ref. 3 but additional information has been obtained by schlieren photography and the present tests extend the range of conditions considered as well as examining the leeside flow in greater detail.

2. Experimental Technique

2.1 Wind Tunnel and Instrumentation

2.1.1 Wind Tunnel

All tests were made in The Hatfield Polytechnic 200mm x 225mm blowdown supersonic wind tunnel (Ref. 4) at a Mach number of 2.5. This tunnel is of conventional design supplied with air from storage tanks, and consequently there is a change in Reynolds number during a run due to the reduction in stagnation temperature as the run proceeds. All quoted Reynolds numbers thus refer to a mean value during a run and typically the variation from this mean value is in the order of 15%.

2.1.2 Pressure and Temperature Measurement

The tunnel stagnation and model static pressures were measured using unbonded strain gauge transducers coupled to a data acquisition system based on a DEC 11/03 computer (Ref. 5). The tunnel stagnation temperature was measured using a platinum resistance thermometer situated in the settling chamber.

2.1.3 Schlieren System

A conventional single pass schlieren system was used, with a quartz halogen light source. The knife edge was usually used in the horizontal position in order to render the boundary layer visible.

2.1.4 Oil Flow

Surface oil flow patterns were obtained by using a lamp black/kerosene mixture on the cylindrical surface. After a run the model was rolled on to transparent adhesive tape to obtain a picture of the flow on the developed cylindrical surface. The tape was then stuck to white paper and the flow pattern recorded using a standard photocopying machine.

2.2 Model and Shock Wave Generator

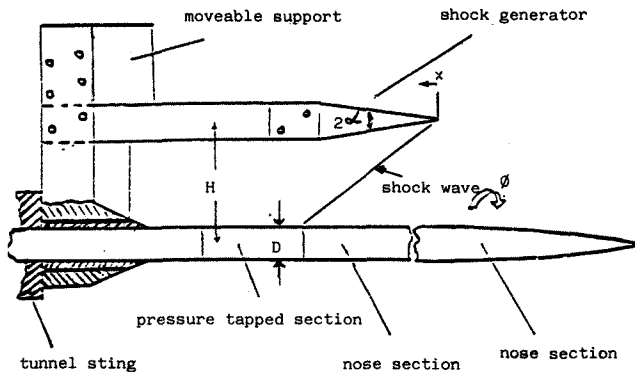The general arrangement of the model and shock wave generator are shown in Figure 1.

FIGURE 1 — CYLINDER AND SHOCK WAVE GENERATOR

2.2.1 Design of Model Nose and Afterbody

It was required that the flow in the region of the shock wave intersection should be influenced by the nose region of the model as little as possible. For this reason, a relatively long nose section was used, a tangent ogive form being chosen for relatively simple manufacture. The length/diameter ratio of the nose was selected in the light of theoretical predictions using a non-homentropic characteristics method (Ref. 6) combined with a conical flow routine (Ref. 7). The final length/diameter ratio of 15:1 was sufficient to ensure small flow variations in the region of the pressure measurement section on the afterbody (typically of the order of 2% in surface pressure) while at the same time avoiding excessive error due to slight misalignment of the model with the local flow direction in the wind tunnel.

Between the tangent ogive section and the pressure measurement section, where the shock wave impingement took place, a further parallel section could be inserted or removed. This allowed the influence of the nose section to be checked experimentally and also provided a means of changing the boundary layer thickness in the intersection region.

The measurement section (Fig. 1) was fitted with three lines of pressure tappings (0.25mm in diameter) and the model could be rotated about its axis in order to provide adequate resolution of the pressure distribution in the rolling direction. The total number of tappings that could be employed was restricted by the available space in the lead out from the tunnel sting.

2.3 Shock Wave Generator

The shock wave generator (Fig. 1) was made with alternative wedges giving flow deflection angles of 6°, 9.5° & 13°. In order to limit the normal force acting on the wedge during a run, a symmetrical wedge was used. The mounting assembly was capable of longitudinal and lateral motion relative to the model in order to vary the impingement area of the shock wave with respect to the pressure measurement section. Originally, it was hoped to employ a two dimensional wedge spanning the tunnel to avoid the tip flow on the wedge being visible in the schlieren photographs. However, blockage and starting load considerations led to a wedge of reduced span to relieve these problems while, at the same time, keeping the tip Mach cones clear of the measurement section.

3. Reynolds Number and Boundary Layer State

The unit Reynolds number of the tests was 37.1×10^6, compared with 18.2×10^6 in Ref. 3. The Reynolds number, based on distance from the nose of the model, was thus 12×10^6 for the long nosed model and 6.46^6 for the short nosed model.

The boundary layer conditions on the cylindrical afterbody, immediately before the intersection region, are clearly of importance. Because of the small scale of the experiment, it was difficult to obtain direct measurements within the boundary layer, apart from the schlieren observations. Consequently, a theoretical method was used to gain insight into the boundary layer state.

The theoretical method used was the second computational method of Walz (Ref. 8) as this was applicable to the Reynolds and Mach number ranges considered. In all the tests the boundary layer was turbulent and the thickness immediately prior to the shock wave interaction was calculated to be 5mm for the long nose and 2mm for the short nose. The corresponding thickness for Ref. 3 was 12.2mm.

4. Discussion of Results

4.1 Windward Region

On the windward side of the cylinder (i.e. the region nearest to the shock wave generator) the flow is characterized by a severe crossflow. This can be clearly seen from the oil flow (Fig. 2). The shock wave reflects from the cylinder surface, the strength of the reflection being greatest at the point nearest to the shock generator and reducing to zero at $\emptyset = 90°$.
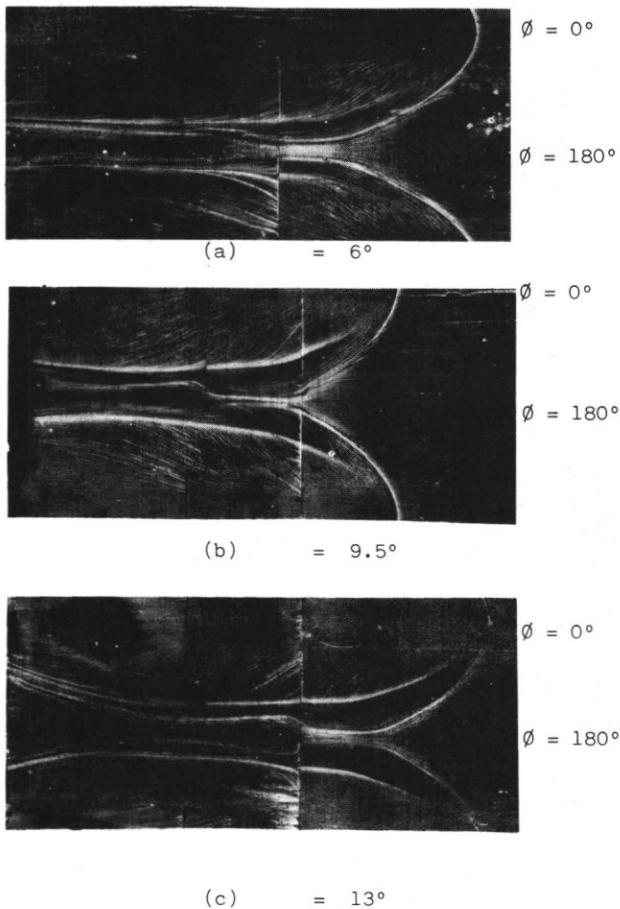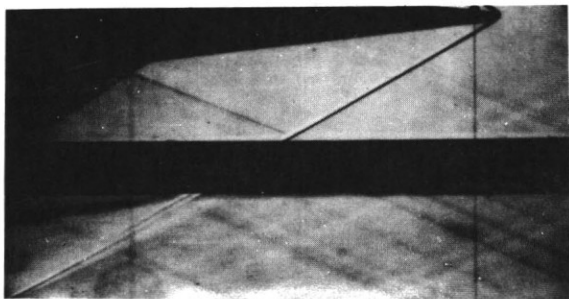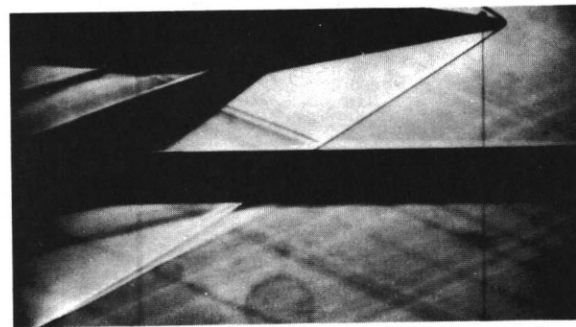
This can be seen in the pressure distributions

(a) = 6°

(b) = 9.5°

(c) = 13°

FIGURE 2 - SURFACE OIL FILM

(e.g. Fig. 4). The strong lateral pressure gradient from $\emptyset = 0°$ to $\emptyset = 90°$ causes the cross flow mentioned above.

The nature of the shock wave reflection depends upon the strength of the incident shock and the state of the boundary layer immediately upstream of the intersection line. In Ref. 3, three distinct types of separation are identified in this region. For the stronger incident shock waves a double separation bubble is obtained while for the weaker incident shock only one

(a) = 6°

(b) = 9.5°
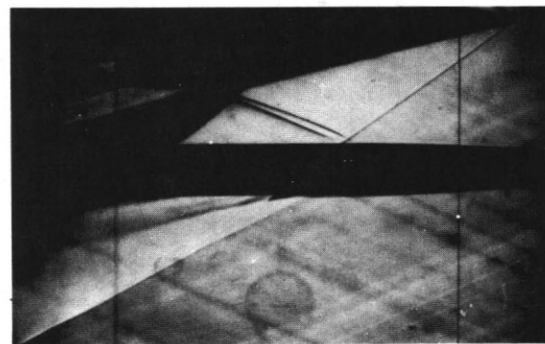
(c) = 13°

FIGURE 3 - SCHLIEREN PHOTOGRAPHS

bubble is observed. In all cases, two reflected shock waves are indicated by the surface pressure distributions. In the present test, a single bubble was obtained in all cases, and for the weakest incident shock wave (corresponding to a wedge deflection of 6°) only a single reflected shock wave was obtained. This can be seen in both the pressure distributions (e.g. Fig. 4) as well as the schlieren photograph, Fig. 3(a). In all other cases, the two reflected waves were present with an expansion wave between, as shown in Figs. 3(b) and 3(c) and, schematically, in Fig. 5.
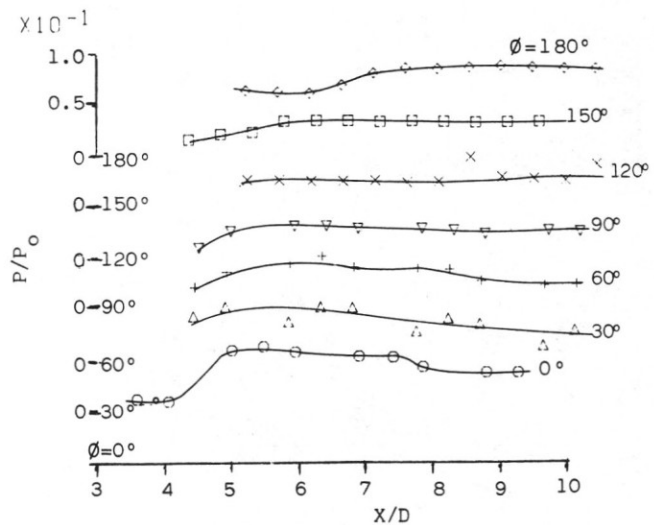

FIGURE 4 (a) α = 6°

1164

$\times 10^{-1}$

P/P$_0$

(b) $\alpha = 9.5°$

$\times 10^{-1}$

P/P$_0$

(c) $\alpha = 13°$

FIGURE 4 - PRESSURE DISTRIBUTIONS

a Incident shock wave   b Reflected shocks
c Separation line   d Expansion
e Expansion from wedge   f Vortex
g Separation bubble
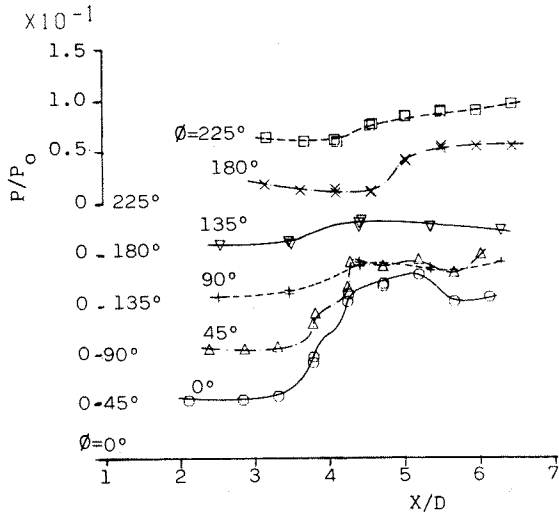

FIGURE 5 - MAIN FEATURES OF FLOW FIELD

4.2 Leeward Region

On the leeward side of the cylinder ($\emptyset > 90°$) the crossflow described above interacts with the oncoming stream parallel to the cylinder axis to produce a somewhat stronger shock wave than the original incident wave. This results in the typical distorted wave which is visible in the schlieren photographs.

For the conditions of Ref. 3 the shock waves on each side of the cylinder meet in a regular intersection, making an angle to the free stream which is greater than the Mach angle. Downstream of the intersection point, the transmitted shock waves return the stream to the axial direction (as required by symmetry at $\emptyset = 180°$). This region appears to be terminated by a normal shock wave.
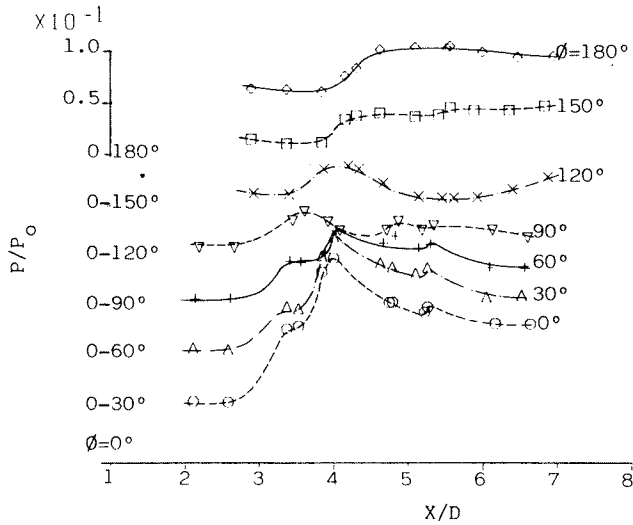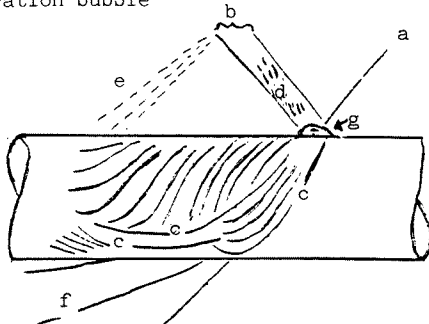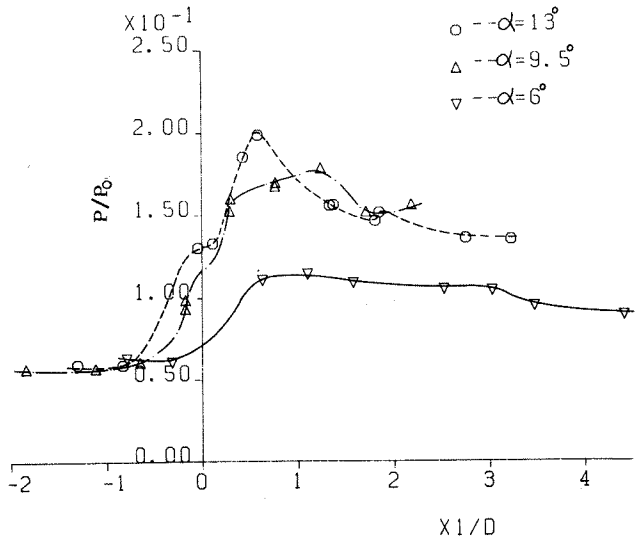
The present investigation revealed a somewhat different mechanism in this region. It can be seen in the surface oil film pictures that the traces associated with the shock waves do not, in fact, meet in this region. The surface pressure distribution (Fig. 4) when combined with the corresponding oil film (Fig. 2), indicates that an embedded patch of near normal shock wave occurs, producing a Mach type intersection at $\emptyset = 180°$.

Downstream of this a pair of vortices are present, as indicated both in the schlieren photographs (Fig. 3a), and by the oil film which shows an outflow meeting the cross flow in a separation line.

4.3 Pressure Distributions

FIGURE 6 - UPSTREAM INFLUENCE OF SHOCK AT $\emptyset = 0$

In Fig. 6 a compairson of the pressure distributions at $\emptyset = 0°$ is made for the three incident shock strengths. The origin of x in this figure is taken at the intersection point of the incident shock wave with the cylinder, determined from the

schlieren photographs. As well as enabling a comparison to be made of the pressure increase caused by the intersection, the extent of the influence transmitted upstream through the boundary layer is shown.
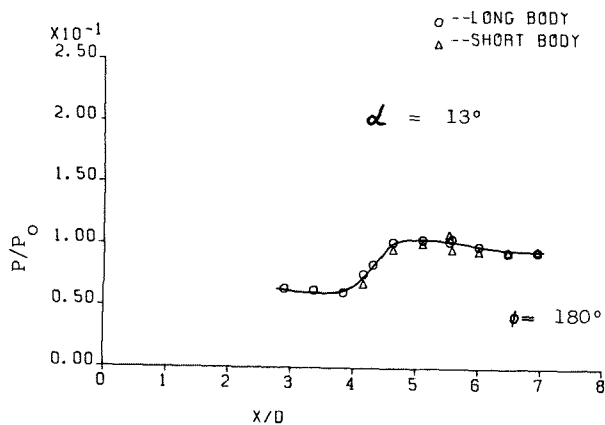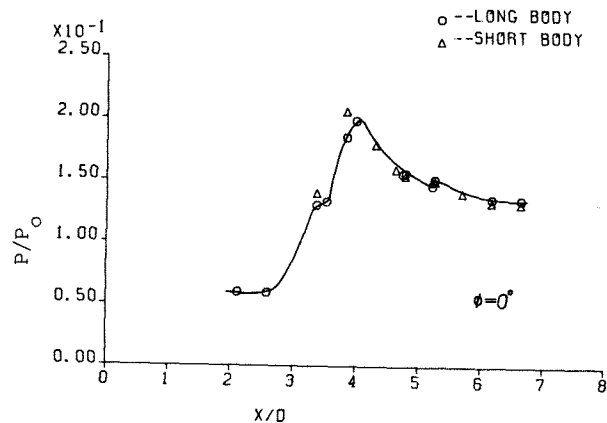

FIGURE 7 – COMPARISONS BETWEEN LONG
AND SHORT NOSES

Figs. 7(a) and 7(b) show that the pressure distributions for the long and short nosed models are substantially the same, and are therefore not significantly influenced by the change in boundary layer thickness between one case and the other.

The effect of the height of the wedge above the cylinder is shown in Fig. 8. As would be expected, the position of the pressure peak caused by the intersection moves rearwards as the wedge height is increased. An unexpected feature is the reduction of the magnitude of the pressure rise with increasing wedge height. A corresponding change in the separation pattern is also reported in Ref. 3. Since the wedge tip flows should have no influence, presumably the effect is caused by the closer proximity of the following expansion wave to the incident shock. The influence of this expansion could, through the boundary layer, modify the separation bubble downstream of the shock intersection point.
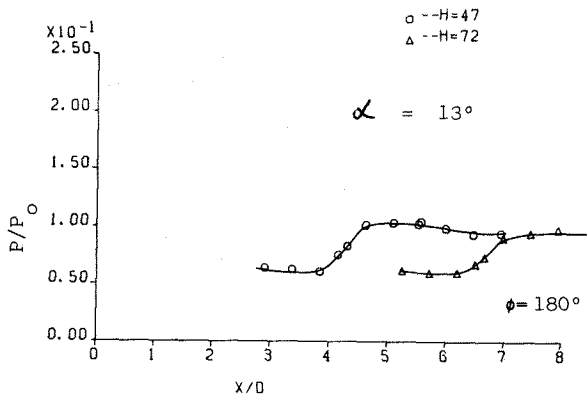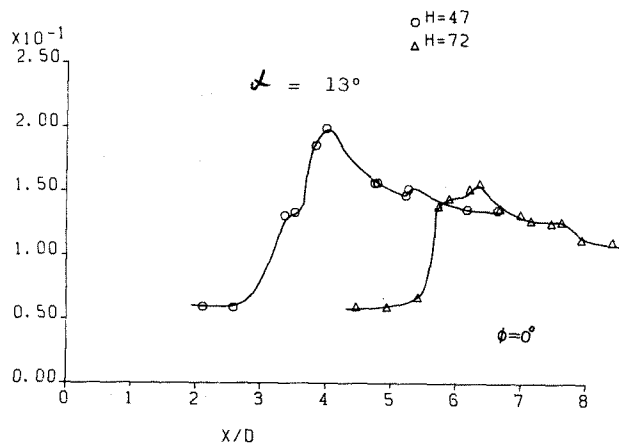
FIGURE 8 – INFLUENCE OF WEDGE/CYLINDER
LATERAL SEPARATION

Figs. 4(a) to 4(c) indicate that the pressure distributions in the windward region ($\emptyset$ = 0 90°) are similar to those of Ref. 3, except that for the weakest incident shock wave only one reflected shock wave is indicated (Fig.3(a)) as mentioned above. The distance over which the increased pressure caused by the shock impingement persists downstream is considerably greater than indicated in Ref. 3. This is because the expansion wave generated by the trailing edge of the wedge strikes the cylinder further downstream since, in the present tests, attempts were made to extend the region unaffected by the expansion as much as possible.

The same figures show that the leeward pressure rise ($\emptyset$ = 90° to 180°) indicates the presence of a shock wave at all values of $\emptyset$, including $\emptyset$ = 180° and this is consistent with the existence of a Mach type interaction in this region. In this case, however, the "bridging" shock wave must be oblique, as is indicated by the schlieren photographs, since it is comparatively weak.

This, in turn, indicates the existence of
a separation, since the shock wave must
produce a deflection away from the surface
at $\emptyset = 180°$ if it is oblique.

5.   Conclusions and Future Work

The flow associated with the type of inter-
section considered is characterized by a strong
crossflow induced by the lateral pressure
gradient downstream of the shock wave inter-
section.

In the cases tested, including those of
Ref. 3, there are some differences in windward
separation patterns and in the leeside flow,
where further investigation is required.

Changing the boundary layer thickness by
shortening the nose was found to have little
effect on the flow.

In order to investigate further the effect
of the boundary layer on the interaction process,
a suction model is currently being constructed
to enable the boundary layer to be removed
immediately upstream of the shock intersection
region.

6.   References

1 Edney B   Anomalous heat transfer and
   pressure distributions on blunt bodies at
   hypersonic speeds in the presence of an
   impinging shock.
   FFA Rt 115 196B

2 Philpott D R and Zhao J Z   Interference
   effects between spherically blunted
   cylinders at M = 2.5 and 1.5.
   AIAA paper 84 2098 1984

3 Brosh A, Kussoy M I and Hong C M   Experi-
   mental and numerical investigation of shock
   wave impingement on a cylinder.
   AIAA Journal Vol. 23 No. 6 1985

4 Preston N O et al   Proposed 9" x 8" super-
   sonic wind tunnel for Hatfield College of
   Technology.
   BAe (Guided Weapons Division) 1964

5 Philpott D R   Pressure measurement in a
   blow down wind tunnel.
   Use of Micros in Fluids BHRA 1983

6 Philpott D R   A program for the calculation
   of axisymmetric supersonic flows around
   blunt bodies using a reference plane method.
   The Hatfield Polytechnic THP/75R 1975

7 Jones D J   Numerical solution of the flow
   field for conical bodies in a supersonic
   stream.
   National Research Council of Canada
   Report LR-507 1968

8 Walz A   Boundary layers of flow and heat
   transfer.
   MIT Press 1969 p 135 ff